

Optics Letters

Low-loss, low-background aluminum oxide waveguide platform for broad-spectrum on-chip microscopy

FIREHUN T. DULLO,^{1,*} NIKHIL JAYAKUMAR,² MICHAEL GETZ,¹ AINA K. HERBJØNRØD,¹ CHRISTOPHER A. DIRDAL,¹ DANIEL NILSEN WRIGHT,¹ FRØYDIS S. SKOTTVOLL,¹ SIRAWIT BOONSIT,³ GANAPATHY SENTHIL MURUGAN,³ DAND BALPREET S. AHLUWALIA² D

Received 26 December 2024; revised 17 February 2025; accepted 20 February 2025; posted 21 February 2025; published 18 March 2025

A versatile wide-spectrum photonic integrated circuit (PIC) platform, spanning from ultraviolet (UV) to infrared (IR) wavelengths, is essential for advancing on-chip optical microscopy and spectroscopy applications. The key desirable requirements for PICs are low-loss, low-autofluorescence background signals, and high-refractive index contrast (HIC) to enable compact designs. Here, we present a low-loss, low-autofluorescence aluminum oxide (Al₂O₃) waveguide platform developed using atomic layer deposition (ALD). At 405 nm, the Al₂O₃ strip waveguide exhibits an autofluorescence background approximately 200 times lower than silicon nitride (Si₃N₄) and a propagation loss of less than 0.5 dB/cm. We demonstrate the suitability of the Al₂O₃ platform for multicolor on-chip total internal reflection fluorescence (TIRF) and super-resolution optical microscopy. The proposed Al₂O₃ platform offers a promising solution for highly sensitive on-chip bioimaging and spectroscopy applications.

© 2025 Optica Publishing Group under the terms of the Optica Open Access Publishing Agreement

https://doi.org/10.1364/OL.551736

Photonic integrated circuits (PICs) enable the integration of multiple optical components with diverse functionalities into compact footprints, enabling efficient light engineering and manipulation [1]. The PIC for the infrared spectrum is well-established and primarily based on silicon as the core material. However, silicon is only transparent above 1.1 μ m, limiting the use of silicon-based PICs for shorter wavelengths in the visible and UV spectrum. Consequently, alternative materials with transmission windows extending into the visible and ultraviolet (UV), such as silicon nitride (Si₃N₄) [2], tantalum pentoxide (Ta₂O₅) [3], lithium niobate (LiNbO₃) [4], aluminum nitride (AlN) [5], and aluminum oxide (Al₂O₃) [6,7], have been explored. The PICs supporting the visible spectrum have found applications in various fields such as on-chip optical microscopy

[8] and spectroscopy [9], offering both miniaturization and also integration of multiple modalities, thereby enhancing imaging and sensing performance.

Low-background signal is essential for high-sensitivity onchip microscopy and spectroscopy, such as single-molecule localization microscopy (SMLM) [8], total internal reflection fluorescence microscopy (TIRF) [10], label-free imaging based on cell or tissue autofluorescence [11–13], Raman spectroscopy [14], and UV spectroscopy [15]. Notably, autofluorescencebased label-free imaging and on-chip UV spectroscopy further require platforms capable of operating effectively within the UV and visible spectrum

Currently, on-chip microscopy and spectroscopy platforms are based on Si_3N_4 [3], Ta_2O_5 [14], and LiNbO₃ [4]. While these platforms are functional and widely adopted, they have inherent limitations, including high propagation losses at the lower end of the visible spectrum (e.g., 405-450 nm). Furthermore, a recent comparative study of the background signals from Si₃N₄ and Ta₂O₅ has revealed that Si₃N₄ exhibits strong background signal, whereas Ta2O5 has exhibited significantly lower background signal [3]. The advantage of low-background signal was highlighted in SMLM [3], where the Ta₂O₅ platform achieved superior single-molecule localization compared to the Si₃N₄ platform. Similarly, in resonance Raman spectroscopy [14], the low-background signal of the Ta₂O₅ platform was crucial for high-sensitivity detection. However, a high-loss and a high background signal limit the practical utility of Ta₂O₅ and Si₃N₄ platforms below 450 nm for microscopy and spectroscopy applications.

Development of wideband (250–1000 nm) PIC, with low optical loss and low-background signal, is critical to fully unlock the potential of the PIC technology for on-chip microscopy and spectroscopy. To cater these needs, Al₂O₃ based PIC appeared as a promising candidate, demonstrating functionality in both the visible and UV spectra [12,16]. For instance, Al₂O₃ based PIC has been employed in far-field UV autofluorescence microscopy [12], guiding UV light at 360 nm and coupling it out of the

¹SINTEF Digital Dept. of Microsystems and Nanotechnology, Gaustadallen 23C, 0373 Oslo, Norway

²UiT The Arctic University of Norway, Klokkargårdbakken 35, 9037 Tromsø, Norway

³Optoelectronics Research Center, University of Southampton, Southampton S017 IBJ, UK

^{*}firehun.t.dullo@sintef.no

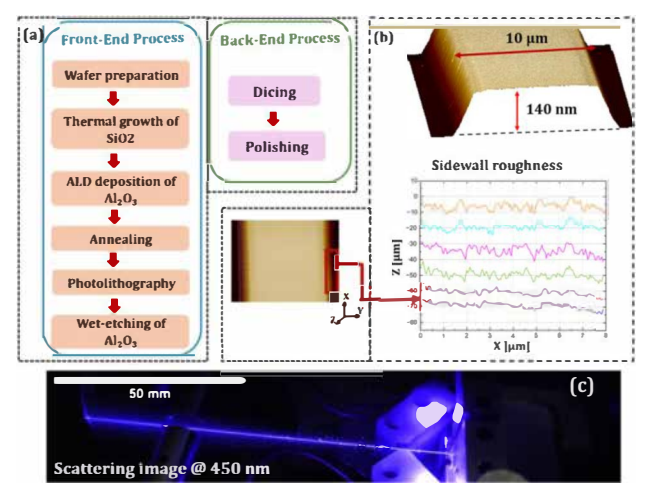


Fig. 1. (a) Front and back-end processes for producing an Al_2O_3 PIC platform. (b) AFM image of a $10\,\mu m$ wide and $140\,nm$ thick strip waveguide and the sidewall roughness measurements. (c) Picture showing light guidance in an Al_2O_3 slab waveguide illuminated with a $450\,nm$ wavelength.

chip to generate structured illumination patterns in the farfield. Despite its promise, Al_2O_3 based PIC remains relatively unexplored. Optimizing their fabrication process and understanding the background signal characteristics across the visible spectra are important next steps toward establishing the platform for microscopy and spectroscopy applications.

In this study, we investigate the optical losses and the background signal of Al₂O₃ platforms deposited using atomic layer deposition (ALD) with various oxygen precursors. Using both H₂O and O₃ as oxygen precursors has previously shown reduced permeability [17], as well as improved surface passivation compared to using only one of them (i.e., only H₂O or only O₃) [18]. This improvement may result from a reduced concentration of carbon and hydrogen when both precursors are used, rather than either one alone [18]. We evaluate the impact of post-deposition annealing, which has previously been shown to increase film density [19] and chemical stability [20]. The background signal of Al_2O_3 are compared to the commonly used Si₃N₄ and Ta₂O₅ within the visible spectrum to assess their viability for high-sensitivity, broad-spectrum applications. Finally, we demonstrate multicolor on-chip optical microscopy, validating the Al₂O₃ platform's potential for bioimaging.

The fabrication steps utilized in this work to produce Al_2O_3 based PIC is illustrated in Fig. 1(a). A 2.5 μ m SiO₂ isolation layer is thermally grown by wet oxidation on a silicon wafer substrate to prevent optical leakage. The Al_2O_3 layer is then deposited by thermal ALD in a Piscosun P-300B reactor, using electronic-grade trimethylaluminium (TMA), DI-H₂O, and/or O₃ as precursors, with a N₂ purge between each pulse. H₂O and O₃ are pulsed in sequence when both are used. One wafer from each deposit received annealing at 435°C for 30 min in forming gas (95% N₂, 5% H₂).

To fabricate channel and strip waveguides, the waveguide structures were defined through photolithography, followed by selective wet etching of Al_2O_3 using phosphoric acid (H_3PO_4). The sidewall roughness, a primary source of propagation loss, was reduced by optimizing the wet etching process. An

Table 1. Experimental Details of the ALD-Al₂O₃ Thin Film Deposited at 300 °C (Unannealed and Annealed at 435 °C) and the Corresponding Measured Transmission Loss at 450 nm

Sample No.	Precursors	Thickness of Al ₂ O ₃ (nm)	Annealed	Transmission Loss at 450 nm (dB/cm)
1	TMA + H ₂ O	142	No	1.30
2	TMA + H ₂ O	137	Yes	0.45
3	TMA + O ₃	136	No	3.50
4	TMA + O ₃	138	Yes	2.36
5	TMA + H ₂ O + O ₃	143	No	0.55
6	TMA + H ₂ O + O ₃	143	Yes	0.36

AFM image of a $10\,\mu m$ wide and $140\,nm$ thick strip waveguide (Fig. 1(b)) shows a sidewall roughness of $2.2\,nm$ and a top surface roughness of $1.12\,nm$. The wafer was then diced into individual chips and edge-polished to produce smooth, high-quality facets.

Table 1 presents the parameters used for optimization of the transmission loss based on the choice of precursors and annealing. The thickness was determined using spectroscopic ellipsometry (SE), and the transmission loss was measured by a prism coupler, Metricon 2010/M. The minor variation in thickness is not expected to affect the comparison of the transmission loss. A 450 nm excitation laser source in the TE polarization was coupled into the slab waveguide via a prism, with the incident angle of the laser beam carefully optimized to enhance coupling efficiency to the fundamental mode. The propagation loss of the waveguide was determined by analyzing the decay of scattered light along the waveguide length (\sim 5 cm). To minimize the impact of inhomogeneity, losses were averaged across different areas of the 6 in. wafer. The results for films deposited at various conditions are listed in Table 1.

Optical measurements revealed that a $140\,\mathrm{nm}$ alumina layer deposited with $TMA + H_2O + O_3$, and annealed at $425\,^\circ\mathrm{C}$, achieves a transmission loss of $0.36\,\mathrm{dB/cm}$ at $450\,\mathrm{nm}$, with a refractive index of 1.71. An image of the light streak (scattering) at $450\,\mathrm{nm}$ for the alumina slab waveguide is shown in Fig. 1(c), where the light coupling into the slab waveguide (6 in. wafer) was achieved using a prism. The refractive index of the slab waveguide for various precursors is measured using spectroscopic ellipsometry, and the results obtained are shown in Fig. 2. A correlation was observed between the refractive index and transmission loss: the process using only O_3 resulted in the lowest refractive index, while those with both H_2O and O_3 yielded the highest. Annealing resulted in an increased refractive index for all the process variations, indicating increased film density, which correlates with reduced hydrogen and carbon

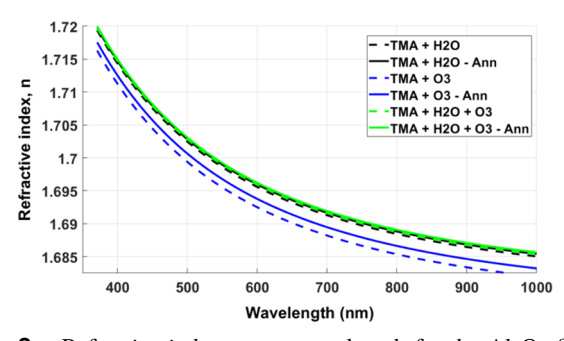


Fig. 2. Refractive index versus wavelength for the Al_2O_3 films investigated in this study.

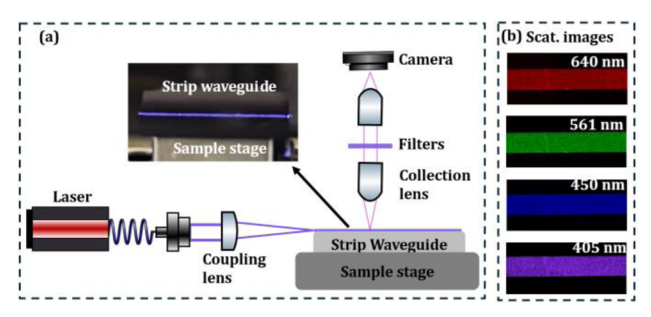


Fig. 3. (a) Schematic sketch of the setup of on-chip microscopy. The same setup was used to measure loss of strip waveguides. (b) Scattering images of a strip Al_2O_3 waveguide illuminated with various wavelengths: 640 (red), 561 (green), 488 (blue), and 405 nm (violet—blue), captured using a $10\times$ collection lens.

impurities. A reduction in these impurities minimizes absorption losses, explaining the link between high-refractive index and lower transmission losses.

Strip waveguides are prone to high sidewall roughness due to their geometry. The propagation losses are also pronounced for the shorter wavelengths as the propagation loss is inversely proportional to the fourth power of wavelength. The propagation loss of the strip waveguides was measured using the setup shown in Fig. 3(a) and quantified using the out-of-plane scattering techniques [21]. The scattering images of the waveguide surface illuminated with different wavelengths (405, 488, 561, and 640 nm) are shown in Fig. 3(b). For a 200 µm wide waveguide, produced using a process similar to that of sample #6 in Table 1, the propagation loss at 405 nm was measured to be below 0.5 dB/cm for both the TE and TM polarizations using the out-of-plane scattering technique [21]. The measured scattered light is directly proportional to the optical power in the guided mode at a given point, encompassing the primary loss mechanisms, including material absorption, radiation leakage, and scattering losses due to surface roughness.

Figure 3(a) depicts an on-chip optical microscopy setup. The chip is held on a sample stage. Laser excitation light (iChrome MLE, TOPTICA Photonics, 100 mW, with wavelengths of 405, 488, 561, and 640 nm) is coupled into a single-mode fiber (P1-460Y-FC-1, Thorlabs) and collimated with a reflective collimator (RC04FC-P01, Thorlabs). A coupling objective lens (Olympus 50×, 0.5 NA) focuses the beam onto the waveguide's end facet. The lens is mounted on an X-Y-Z translation stage, for precise positioning of the laser focus on the input facet using a nanometer-precision stage (Nanomax 300, Thorlabs). Focus adjustments and mode patterns inside the waveguide can be made with a piezo controller (MDT693B Open-Loop Piezo Controller, Thorlabs) for piezo-based scanning. Fluorescent light emitted by the sample on the waveguide is collected by an upright objective lens and filtered through long pass and bandpass filters (BLP02-561R-25, Stock#67-034; BLP01-664R-25, FF01-692/40-25, Semrock) to block excitation light before imaging onto a CMOS camera (ORCA-Flash4.0 v2,).

Using the optical setup shown in Fig. 3(a), the autofluorescence background signal of the Al_2O_3 waveguide platform was measured and compared with the widely used Si_3N_4 and Ta_2O_5 waveguides. To investigate the autofluorescence, the waveguide was illuminated by the end facet coupling. The images were captured using an upright microscope, with different combinations of long and bandpass filters for each wavelength. The

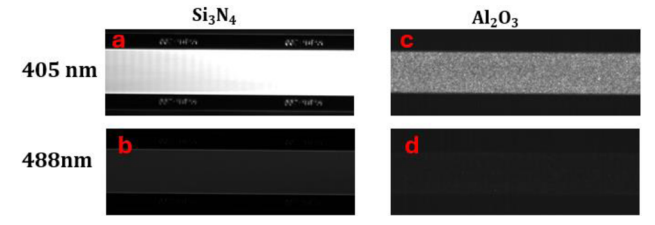


Fig. 4. Background signal imaged with waveguide excitation for different platforms and excitation wavelengths, (a), (b) Si_3N_4 waveguide and (c), (d) Al_2O_3 waveguide. All images are approximately 975 μ m by 390 μ m.

Table 2. Background Signal from Al_2O_3 , Si_3N_4 , and Ta_2O_5 Waveguide Platforms for Different Excitation Wavelengths^a

Wavelength (nm)	Al_2O_3 BG Counts	Si_3N_4 BG Counts	Ta ₂ O ₅ BG Counts
640	100*	152	100*
561	100*	386	100*
488	100*	614	100*
405	124	4800	-

"The camera used for the experiments has an offset of 100 counts. BG = background.

filters blocked the coupled light and collected only the autofluorescence emissions from the waveguide surface, following the approach described by Coucheron et al. [3]. The autofluorescence background was quantified by subtracting the mean pixel counts of the waveguide surface from the camera background. Identical experimental conditions including input power (100 mW), acquisition time (100 ms), and chip design were used to ensure a fair comparison of the autofluorescence backgrounds. The results, shown in Fig. 4 and detailed in Table 2, demonstrate that the Al₂O₃ and Ta₂O₅ waveguides exhibited no measurable autofluorescence using our instruments at 488, 561, and 640 nm. A minimal autofluorescence was observed for the Al₂O₃ waveguide at 405 nm, which was approximately 200 times less than that of the Si₃N₄ waveguide at the same wavelength. Ta₂O₅ used here exhibited a high loss at 405 nm and thus could not guide light at this wavelength, preventing reliable measurement.

The fabrication details of Si_3N_4 and Ta_2O_5 used in this study are consistent with those described in our previous work [3].

Next, we demonstrated the utility of the Al₂O₃ waveguide platform for multicolor on-chip TIRF microscopy. HeLa cells were seeded on the waveguide platform inside a polydimethylsiloxane (PDMS) chamber and then placed inside an incubator at 37°C. After 24 h, the waveguide chips were removed, and the cells were fixed with 4% paraformaldehyde (PFA) for 10 min at room temperature. The fixed cells were washed three times with phosphate-buffered saline (PBS), and then the cell membrane was permeabilized using 0.1% Triton X-100 at room temperature. Actin filaments were stained with Phalloidin-Atto 647N dye, prepared as a 1:50 dilution in PBS. After 10 min, the cells were gently rinsed three times with PBS. The nuclei were stained with DAPI (Thermo Fisher Scientific), diluted in 1:1000 PBS, and rinsed another three times with PBS after 10 min. Finally, the chips were sealed with #1.5 coverslips for imaging. Figure 5 shows the on-chip TIRF imaging of nucleus and actin filaments using the Al₂O₃ waveguide. Here, we utilized the super-resolution method based on auto-correlation two-step deconvolution (SACD [22]). First, an image stack of 300 frames was acquired by scanning the laser beam at the end facet of the

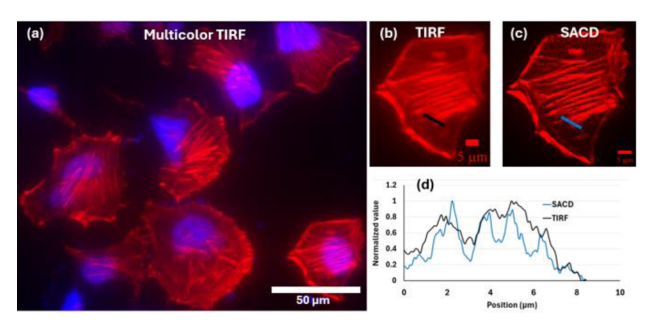


Fig. 5. Demonstration of an Al_2O_3 waveguide for (a) multicolor imaging of actin and nucleus in fixed HeLa cells. The images are acquired using a water immersion objective lens (60×, 1.2 NA). (b) TIRF images were obtained by averaging a stack of images and (c) super-resolution images are obtained using SACD. (d) Improvement in resolution by SACD is demonstrated by the line profile along areas shown by the black and red lines highlighted in (c).

waveguide [8]. A TIRF image was then obtained by averaging the image stack, while a super-resolved image was obtained by processing the image stack in SACD (Fig. 5(c)). The presence of any background autofluorescence signal would have generated imaging artifacts using the SACD algorithm.

We have utilized ALD to fabricate a low-loss and low-background Al_2O_3 PIC platform optimized for the entire visible spectrum. The measurements revealed that the Al_2O_3 platform exhibits significantly lower background signal approximately 200 times lower at 405 nm compared to the Si_3N_4 platform. Furthermore, the Al_2O_3 platform achieved the lowest propagation loss of 0.36 at 450 nm and 0.5 dB/cm at 405 nm for the slab and strip waveguides, respectively, outperforming both Si_3N_4 and Ta_2O_5 at this wavelength.

Furthermore, we demonstrated the Al_2O_3 platform's compatibility for multicolor on-chip optical microscopy by imaging fixed HeLa cells. The results highlight the platform's ability to support multicolor bioimaging, including visible wavelength, such as 405 nm, which remains challenging with the presently used waveguide platforms. The combination of low-background signal in the visible and NIR spectrum and low optical loss spanning from the UV to the near-infrared (NIR) spectrum makes the Al_2O_3 platform a highly promising candidate for a variety of advanced photonic applications.

Funding. HORIZON EUROPE Framework Programme (101135796); HORIZON EUROPE European Innovation Council (101058016).

Acknowledgment. The authors acknowledge the contributions from Erik Poppe (SINTEF Digital, Oslo, Norway), Vishesh K. Dubey and Hong Mao (UiT-The Arctic University of Norway), and Vetle Øversjøen (SINTEF Industri, Oslo, Norway).

Disclosures. B.S.A. has applied for patent for chip-based super-resolution microscopy and is the co-founder of the company Chip NanoImaging AS, which commercializes on-chip super-resolution microscopy. All other authors declare no conflicts of interest regarding this article.

Data availability. Data underlying the results presented in this article are not publicly available at this time but may be obtained from the authors upon reasonable request.

REFERENCES

- S. Y. Siew, B. Li, F. Gao, et al., J. Lightwave Technol. 39, 4374 (2021).
- T. Sharma, J. Wang, B. K. Kaushik, et al., IEEE Access 8, 195436 (2020).
- D. A. Coucheron, ØI Helle, J. S. Wilkinson, et al., Opt. Express 29, 20735 (2021).
- 4. B. Desiatov, A. Shams-Ansari, M. Zhang, et al., Optica 6, 380 (2019).
- 5. N. Li, C. P. Ho, S. Zhu, et al., Nanophotonics 10, 2347 (2021).
- G. N. West, W. Loh, D. Kharas, et al., APL Photonics 4, 026101 (2019).
- W. Hendriks, M. Dijkstra, S. Mardani, et al., in Integrated Optics: Devices, Materials, and Technologies XXVII, S. M. García-Blanco and P. Cheben, eds. (SPIE, 2023), p. 2.
- 8. R. Diekmann, Øl Helle, C. I. Øie, et al., Nat. Photonics 11, 322 (2017).
- S. Nezhadbadeh, A. Neumann, P. Zarkesh-Ha, et al., Opt. Express 28, 24501 (2020).
- J.-C. Tinguely, Øl Helle, and B. S. Ahluwalia, Opt. Express 25, 27678 (2017).
- S. Bhattacharjee, S. Satwaha, K. Thornton, et al., ACS Omega 3, 5926 (2018).
- C. Lin, J. S. D. Peñaranda, J. Dendooven, et al., Nat. Commun. 13, 4360 (2022).
- F. Ströhl, D. L. Wolfson, I. S. Opstad, et al., Light Sci. Appl. 12, 56 (2023).
- D. A. Coucheron, D. N. Wadduwage, G. S. Murugan, et al., IEEE Photonics Technol. Lett. 31, 1127 (2019).
- T. Sarwar, "On-chip UV/VIS optical spectrometer," Ph.D. thesis, (University of Michigan, 2023).
- M. M. Aslan, N. A. Webster, C. L. Byard, et al., Thin Solid Films 518, 4935 (2010).
- 17. M. Li, D. Gao, S. Li, et al., RSC Adv. 5, 104613 (2015).
- G. Von Gastrow, S. Li, M. Putkonen, et al., Appl. Surf. Sci. 357, 2402 (2015).
- G. Dingemans, F. Einsele, W. Beyer, et al., J. Appl. Phys. 111, 093713 (2012).
- M. Broas, O. Kanninen, V. Vuorinen, et al., ACS Omega 2, 3390 (2017).
- S. M. Lindecrantz and O. G. Helleso, IEEE Photonics Technol. Lett. 26, 1836 (2014).
- 22. W. Zhao, J. Liu, C. Kong, et al., "Faster super-resolution imaging with auto-correlation two-step deconvolution," arXiv (2018).